


Confinement highlights the different electrical transport mechanisms prevailing in conducting polymers

Sukanya Das ¹, Anil Kumar,² and K. S. Narayan^{1,*}

¹*Chemistry and Physics of Materials Unit and School of Advanced Materials, Jawaharlal Nehru Centre for Advanced Scientific Research, Bengaluru 560064, India*

²*Department of Chemistry, Indian Institute of Technology Bombay, Powai, Mumbai 400076, India*

 (Received 11 November 2020; revised 19 December 2021; accepted 18 January 2022; published 8 February 2022)

We study the differences in electrical charge transport dynamics of the conductivity enhancement of poly(3,4-ethylenedioxythiophene) (PEDOT) derivatives under geometrical confinement. The results of polymer blend poly(3,4-ethylenedioxythiophene):poly(styrenesulfonate) and a polymer-monomer blend, poly(3,4-ethylenedioxythiophene):tosylate, highlight the role of dopants and processing conditions of these systems under confinement. The prevailing transport length scales in confined geometry of characteristic dimensions originate from varying disorder in these polymer systems. These observable differences in two different PEDOTs introduced by molecular level reorganization can be utilized to tune conducting polymer systems for efficient electrical and thermoelectric properties. The electrical conductivity σ of the polymer system, which is a function of the electronic structure at molecular level and a connectivity parameter, has been probed in cylindrical-alumina nanoscaffolds of various channel diameters, at different frequencies ω and temperatures T . The observations also emphasize the role of disorder in these conducting polymer systems.

DOI: [10.1103/PhysRevMaterials.6.025602](https://doi.org/10.1103/PhysRevMaterials.6.025602)

I. INTRODUCTION

Tuning of the structural organization at different length scales in conducting polymer (CP) blends has helped achieve significant milestones in electrical transport properties. The charge carriers in these CPs traverse different electrical transport regimes ranging from molecular scales to microscopic and mesoscopic length scales. Structural tuning of the appropriate length scale is a key material design tool. Since CPs are inherently disordered and consist of polymer chains with different characteristic lengths and defect distribution, microstructural modifications can alter the transport mechanism significantly [1–6].

With numerous conformational degrees of freedom, the charge transport dynamics varies in different regimes of π -stacked molecular planes. Localization of charges occurs due to the absence of polymer chain ordering over long distances and crystal symmetry. This restricts diffusion of charges and limits the charge transport mechanism to hopping between localized sites, in the framework of the Anderson model [7]. Differences in electronic delocalization length scale within molecular stacks contribute to structural disorder in conjugated polymers. The coexistence of delocalized and localized states in high molecular weight polymers can be interpreted in terms of transport routes and characteristic barriers which act as rate-limiting processes [8]. The transport effectively occurs via intermediate order-disorder pathways of the semicrystalline-amorphous microstructural domains [9]. The properties in the ordered domains set the upper limit for

the charge transport in such heterogeneous microstructures [10]. However, the enhanced σ has also been observed to originate from effective π - π stacking at molecular levels as opposed to contributions solely from improved crystallinity [11]. The rate-limiting factor for charge transport dynamics described by the structure property relation of CPs is thus system specific.

Among the CPs, poly(3,4-ethylenedioxythiophene) (PEDOT) emerges as a versatile candidate with significantly high electrical conductance, thermal and air stability, simple synthesis process, energy storage capacity, optical transparency, and biocompatibility [12–19]. Poly(3,4-ethylenedioxythiophene):poly(styrenesulfonate) (PEDOT:PSS) is an archetypical CP blend where extensive studies have been carried out. The importance of secondary doping processes has been demonstrated for improving σ including solvent-additive introduction, ionic liquids, surfactant treatment, and acid treatment, to name a few [12]. Enhanced σ in PEDOT:PSS has been explained widely in terms of polymer chain alignment emphasizing conformational change from wormlike chains to linear structures [20,21]; electronic and ionic phase separation of PEDOT and PSS, respectively [22]; PEDOT-PSS complex grain size [23]; removal of PSS from PEDOT:PSS grains [24]; and ordering of PEDOT nanocrystals [9,25]. From only a few S/cm to ~ 6000 S/cm, with PEDOT single nanocrystals reaching up to 8797 S/cm [26], the electrical σ of PEDOT is close to that of conventional metals. The other derivative of PEDOT where significant electrical and thermoelectric properties have been observed is poly(3,4-ethylenedioxythiophene):tosylate (PEDOT:Tos), in which a controlled oxidation level during the process of EDOT polymerization in the presence of iron(III)-tosylate has significantly increased the σ [5,27,28]. With the

*narayan@jncastr.ac.in

presence of small nonhindering tosylate counterions and the absence of the long insulating polymer PSS, PEDOT:Tos is more ordered and exhibits metallic transport signatures [16,29]. The wide range of electronic properties prevailing in systems with a common PEDOT backbone is interesting and poses fundamental questions about factors controlling the properties. Specifically, we probe these two contrasting PEDOT systems: PEDOT:Tos and PEDOT:PSS, respectively, in which the *in situ* polymerization in confinement leads to characteristic chain organization, and compare them to the microstructure which is developed upon insertion of another all-polymer blend in the nanocavities. PEDOT chains within such narrow cylindrical cavities offer a test-bed for understanding the structural disorder and its role in electrical transport.

Straight-through hollow alumina nanopores provide rigid, inert, geometrically ordered confinement for these systems. Confined CPs have been previously shown to undergo the general feature of chain alignment accompanied by an enhancement in the conductance. In our previous work [30] we showed that the transverse (nanopore axial) conductivity $\sigma_{\text{transverse}}$ of PEDOT:PSS increases as geometrical confinement increases to 20 nm. In this report, we implement these studies for the *in situ* grown PEDOT:Tos that provides an entirely distinct dopant environment, and highlight the contrasting transport mechanisms upon comparison with that of PEDOT:PSS. The results can be inferred in terms of correlating the polymer chain alignment and role of macromolecular organizational processes for σ to the structural disorder in these low-dimensional templates. These representatives of PEDOT highlight the variation introduced by different dopants on the disorder affecting the extent of delocalization. Previous studies of PEDOT:PSS have shown that the fraction of polarons and bipolarons formed depends on the dopant concentration while in the case of PEDOT:Tos it is predominantly bipolaronic in character [16]. We focus on the domain of chain alignment that maps to the order-disorder boundaries of the polymer blend in the constrained space. It is expected that the molecular rearrangement within nanochannels will result in different ordered phases and extent of their interconnects in the disordered matrix. We investigate the changes in heterogeneous media under confinement and study the response due to small signal electrical perturbation over a wide frequency spectrum and temperature range. The insight gained by confining these systems highlights the order-disorder boundaries and charge dynamics of CPs.

The confinement effect studies are implemented using alumina templates in a film form adhered to a conducting (ITO) substrate. The parallel array of cylindrical pores chosen for the studies are of diameter 20, 50, 80, and 100 nm in the alumina matrix (200 nm thick). The deposition of PEDOT:Tos in the nanochannels involved *in situ* polymerization of the monomer within the alumina scaffold (details in Sec. 1 of the Supplemental Material [31]; also see [32–34]).

Structural studies using x-ray scattering of solution cast polymerized PEDOT:Tos films have indicated a paracrystalline state with sizable anisotropy, where the dopant anions form distinct planes that alternate with stacks of the polymer chains [29]. These films exhibit σ with a metallic behavior in plane and a dielectric behavior out of plane of the films. In the

context of PEDOT:Tos grown in confined anodized aluminum oxide (AAO) nanopores, it is expected that crystallization leads to a preferential orientation. This effect is characteristic of anisotropic crystals, an orientation with the fast-growing crystallographic direction preferring to be along the long axis of the nanopore. An unimpeded growth parallel to the pore axis, especially below a characteristic radial-confinement length scale can be expected. These factors then enable enhancement in transverse conductance of the polymer systems.

II. RESULTS AND DISCUSSIONS

A. Dc transport $\sigma(T)$

Four-probe measurements are carried out to obtain the dc lateral conductivity σ_{lateral} of PEDOT:Tos films of different thicknesses on a variety of substrates. σ_{lateral} [Fig. 1(a)] is obtained to be in the range $\sim 500 (\pm 100)$ S/cm. These values and $\sigma_{\text{lateral}}(T)$ are similar to the reported semimetallic trend of PEDOT:Tos [16]. The $\sigma_{\text{transverse}}$ measured between the bottom ITO electrode and the top Au electrode of the films are observed to be lower than σ_{lateral} by nearly four orders of magnitude, $\sim 10^{-2}$ S/cm. It should be pointed out that $\sigma_{\text{transverse}}$ inhomogeneity has been observed in the case of vapor phase polymerized films [35]. The characteristic of $\sigma_{\text{transverse}} < \sigma_{\text{lateral}}$ can be attributed to the anisotropy of the crystalline segment and the favored interconnected links between the growing crystallites lateral to the amorphous film surface. This scenario is interestingly altered for the nanopore-confined CPs.

The σ of a single PEDOT:Tos nanochannel in the AAO template can be obtained from the $\sigma_{\text{transverse}}$ measurement with knowledge of the pore density; this is possible since PEDOT:Tos fills the alumina pores forming a uniform film. A complete pore filling has been ensured by individually conducting nanopores in conductive atomic force microscopy (CAFM) studies; see the following section and extensive methods mentioned in Sec. 2 of the Supplemental Material [31]. In the present case of the polymer blend confined in alumina nanochannels, $\sigma_{\text{transverse}} (\approx 24 \pm 18$ S/cm) increases by nearly three orders of magnitude as compared to as-cast bulk films ($\approx 10^{-2}$ S/cm) [Fig. 1(b)]. It should be emphasized that the σ_{dc} is obtained after ascertaining the linear $I - V$ characteristics (0–0.8 V), and $\sigma_{\text{transverse}}$ represents σ of a single nanochannel, obtained by normalizing the cumulative response from 10^9 pores/cm². The electrical response from a templated film of $\sim 10^9$ parallel, identical, and well-separated polymer nanopillars can be taken to be an aggregate measure of σ from each nanopore. The pore diameter dependence indicates that $\sigma_{\text{transverse}}$ of the polymers in the nanopores is not a simple scaled magnitude of the bulk $\sigma_{\text{transverse}}$. The pore-induced reconfiguration of the CP chains leads to a significant enhancement of σ and this dramatic nonlinear scaling becomes evident when the geometrical confinement dimensions are comparable to charge transport length scales.

The transport properties of these conducting polymer systems are generally characterized by their degree of disorder which is ascertained from $\sigma_{\text{dc}}(T)$ and the resistivity ratio $\rho_r = \frac{\rho(0 \text{ K})}{\rho(300 \text{ K})}$ [17,36,37]. A higher value of ρ_r corresponds to higher levels of disorder. The $\sigma_{\text{dc}}(T)$ of PEDOT:Tos and

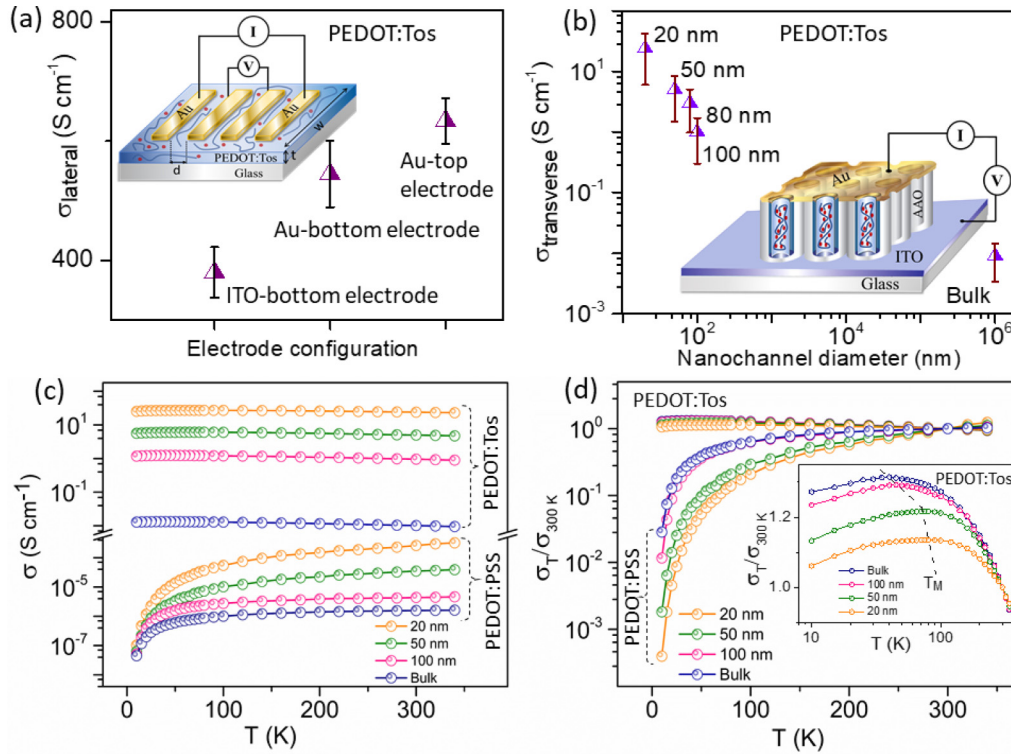


FIG. 1. Dc conduction of PEDOT:Tos: (a) Lateral dc conductivity, σ_{lateral} of PEDOT:Tos films (of thickness 200 nm) for three different configurations of electrode contact on the film with four-probe method on a glass substrate with patterned ITO as bottom electrodes, thermally evaporated bottom Au electrodes, and Au as top electrodes. (b) $\sigma_{\text{transverse}}$ of PEDOT:Tos nanochannels between bottom ITO and top Au electrodes versus polymer filled alumina-nanochannel diameters. Temperature-dependent transverse dc conduction: (c) $\sigma(T)$ of PEDOT:Tos and PEDOT:PSS nanochannels in the temperature range $10\text{ K} < T < 340\text{ K}$ for different channel dimensions and (d) $\sigma_T/\sigma_{300\text{K}}(T)$ (with y axis in log scale) for all PEDOT:Tos and PEDOT:PSS channels; inset shows $\sigma_T/\sigma_{300\text{K}}(T)$ in linear y axis for PEDOT:Tos nanochannel diameters with indication line of the transition temperature T_M .

PEDOT:PSS are studied for different nanochannel dimensions over a range of $10\text{ K} < T < 340\text{ K}$ (Fig. 1(c) and Sec. 5 of the Supplemental Material [31]). The σ_{dc} values for all PEDOT:Tos samples can be extrapolated to a finite magnitude as T approaches zero. The nonzero conductivity indicates the presence of charges in the Fermi level and the possible conduction pathways without any thermal activation. $\sigma_T/\sigma_{300\text{K}}$ versus T is plotted for both PEDOT:Tos and PEDOT:PSS films in Fig. 1(d). In comparison to the PEDOT:PSS samples with a high degree of disorder ($\rho_r \sim 10^3$), the PEDOT:Tos films reveal ordered phases with $\rho_r \sim 1$. The conductivity, $\sigma_{\text{dc}}(T)$, of confined PEDOT:Tos within different channel dimensions shows a negative coefficient of temperature ($\frac{d\sigma}{dT} < 0$) over a wide temperature range above a transition temperature ($T > T_M$). In the range $T < T_M$, $\frac{d\sigma}{dT} > 0$ and $\sigma_{\text{dc}}(T)$ exhibits a weak temperature dependence with a negligible decrease in the magnitude of σ as T is decreased to 10 K. T_M , indicated in the inset of Fig. 1(d), is observed to be a function of the nanochannel diameters (Sec. 5 of the Supplemental Material [31]). Additionally, the high-resolution transmission electron microscopy (HRTEM) images of PEDOT:Tos films show the presence of crystalline PEDOT domains surrounded by amorphous regions (Sec. 6 of the Supplemental Material [31]). These results, however, necessitate a detailed analysis for the structural study of polymer chains in the confined channels.

In comparison, the PEDOT:PSS nanochannels [Fig. 1(c)] show a positive coefficient of temperature throughout the range $10\text{ K} < T < 340\text{ K}$. PEDOT:PSS has been extensively reported to exhibit variable range hopping (VRH) type transport or the nearest neighbor hopping mechanism depending on the film anisotropy [17,38]. The analysis in terms of reduced activation energy is provided in Sec. 5.1 of the Supplemental Material [31]. The decreasing trend of $\sigma_{\text{dc}}(T)$ for PEDOT:Tos in the range $10\text{ K} < T < T_M$ may suggest some of the residual resistances that are typically observed in metallic samples. The nonzero conductivity as $T \rightarrow 0$, improved order parameter in the existing disordered matrix, and $\frac{d\sigma}{dT} < 0$ over wide temperature range suggest a Sheng conduction where fluctuation-induced tunneling [2,5,39] occurs between conducting domains separated by thin insulating ones.

B. Single nanochannel transport

The partially filled PEDOT:Tos nanochannels are locally probed using conductive atomic force microscopy by applying a constant bias voltage between conducting cantilever tip and ITO. It is possible to measure the current magnitude across single channels using the Pt/Ir coated nanoconducting tip which has radius of curvature less than the used pore diameter. The single nanochannel measurements (Secs. 2 and 4 of the Supplemental Material [31]) of PEDOT:Tos reveal a trend similar to that obtained from macroscopic measurements.

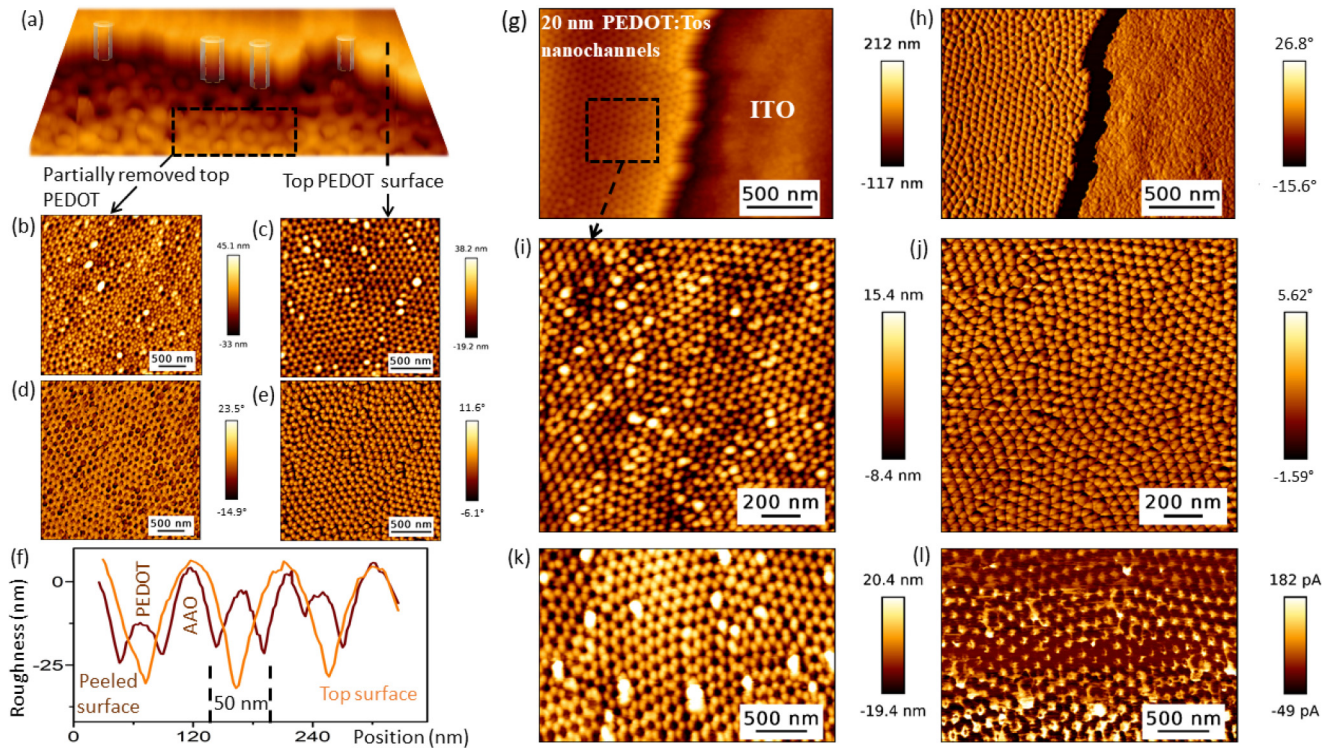


FIG. 2. Single nanochannel transport. (a) Surface morphology of PEDOT:Tos filled 50 nm AAO surface, a section of which is partially removed as indicated by a dotted square region. The resultant cross-sectional image of the interface shows the exposed PEDOT nanopillars, a few of which have color added as a guide. Partial removal of top PEDOT filled AAO surface shows evidence of PEDOT filling through the length of the channels: (b), (d) represents topography and phase, respectively, of the dotted square region which comprises exposed bare alumina and PEDOT filled nanochannels. The alternate bare AAO and PEDOT channels are also shown in the line scan of surface roughness (f) marked in brown. Line scan of surface roughness (f) marked in orange shows a minimum (top concave meniscus of PEDOT adhering to inner surface of nanocylinder formed on annealing) corresponding to each maximum of PEDOT (resultant convex meniscus of PEDOT formed midway of a nanocylinder due to peeling of top PEDOT film) in other line scan marked in brown. (c), (e) are the respective topography and phase images of the top surface of PEDOT filled 50 nm channels. Noncontact mode AFM imaging showing (g), (i) topography and (h), (j) phase across a 20 nm PEDOT:Tos AAO/ITO interface over a scan area of $1.2 \mu\text{m} \times 1.8 \mu\text{m}$ and on a PEDOT:Tos filled 20 nm AAO surface over a scan area of $700 \text{ nm} \times 700 \text{ nm}$, respectively. Conductive AFM in contact mode showing (k) topography and (l) current profile of 80 nm PEDOT:Tos nanochannels.

$I_{20 \text{ nm}} > I_{50 \text{ nm}} > I_{100 \text{ nm}} > I_{\text{bulk}}$ for a constant voltage V has been observed using the same CAFM tip which clearly confirms the nanoconfinement effect. $\sigma_{20 \text{ nm}}$ is three orders of magnitude higher than σ_{bulk} . The analysis process for arriving at conductivity values is similar to our previous work [30] and the relatively minor discrepancy in σ from the two methods reveals the maximum uniformity of PEDOT:Tos across the 10^9 parallel-identical channels.

Figure 2(a) shows a surface image of a top section of 50 nm PEDOT:Tos nanochannels, a portion of which is removed manually by tape exfoliation (details mentioned in Sec. 2 of the Supplemental Material [31]). The partial removal of the top PEDOT layer exposes the polymer filled nanochannels [marked with dotted line in Fig. 2(a)] whose corresponding surface topography and phase images are shown in Figs. 2(b) and 2(d), respectively. The nonexfoliated region has a surface roughness and phase shown in Figs. 2(c) and 2(e). The guide lines in Fig. 2(a) reveal the exposed cross sectional surface scan of 50 nm nanochannels that provides the evidence of the conformal polymer filling within the nanochannels. The details of the complete exfoliation of the

AAO-PEDOT template from the ITO surface is comprehensively presented in Sec. 2 of the Supplemental Material [31]. These results indicate a complete filling of polymer along the length axis of the nanochannels. Figures 2(g) and 2(i) are the surface topography of the 20 nm PEDOT:Tos/ITO interface and a high-resolution $700 \text{ nm} \times 700 \text{ nm}$ scan on an only 20 nm PEDOT:Tos region, while Figs. 2(h) and 2(j) are the corresponding phase images. Figures 2(k) and 2(l) are the topography and current images, respectively, of 80 nm channels. The surface topography, phase, and electric current profiles for the different nanochannel dimensions are shown in Secs. 3 and 4 of the Supplemental Material [31].

C. Ac conduction

The $\sigma(\omega)$ behavior of the alumina-nanopore filled polymer provides useful insight into the carrier dynamics of disordered polymer systems. Changing the dopant environment around the electronic backbone of PEDOT from a long-chain polymer PSS to distribution of small tosylate monomers induces a different length of delocalization of charge carriers and

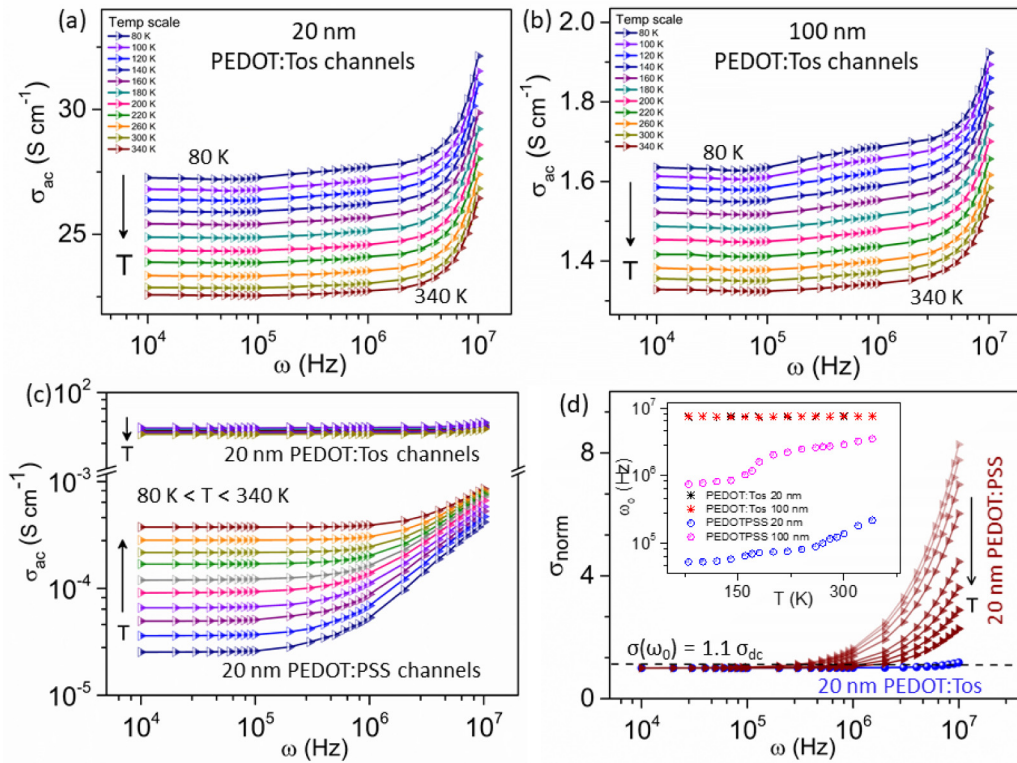


FIG. 3. Ac conduction in (a) 20 nm and (b) 100 nm PEDOT:Tos channels for temperature range $80 \text{ K} < T < 340 \text{ K}$. (c) represents the $\sigma(\omega, T)$ behavior for two polymer blends in 20 nm channels: $\sigma_{\text{PEDOT:Tos}}$ shows a wide dispersion over ω and T scales in comparison to precisely unchanged $\sigma_{\text{PEDOT:PSS}}$. (d) Normalized ac conductivity, σ_{norm} of two polymer blends, PEDOT:PSS (increasingly dark shades of brown in accordance to increasing T scales), and PEDOT:Tos (marked in blue); inset shows the onset frequency $\omega_0(T)$ for PEDOT:PSS and PEDOT:Tos in the range $80 \text{ K} < T < 340 \text{ K}$.

hence the extent of disorder in two polymer blend systems. The prominent highlights of these results [Figs. 3(a) and 3(b)] are the following: (i) $\sigma(\omega)$ of PEDOT:Tos is independent of ω in $10 \text{ kHz} < \omega < 1 \text{ MHz}$ over $80 \text{ K} < T < 340 \text{ K}$ range; (ii) in the high ω region, $1 \text{ MHz} < \omega < 10 \text{ MHz}$, and the $80 \text{ K} < T < 340 \text{ K}$ regime, a weak ω dependence emerges and is described by a power-law frequency dependence of conductivity, $\sigma \sim \omega^s$ where $0 < s < 0.07 (\pm 0.035)$. The variation of exponent s remains nearly constant for all PEDOT:Tos nanochannels ($\sigma(\omega, T)$ of other AAO channels are shown in Sec. 7 of the Supplemental Material [31]). On the other hand, for PEDOT:PSS [Fig. 3(c)], the range of exponent is $0 < s < 0.89 (\pm 0.38)$ and shows a wide dispersion of $\sigma(\omega)$ over the T range. The results of $\sigma(\omega)$ for PEDOT:Tos highlight the weak dependence of σ on ω and T as compared to that of PEDOT:PSS. Normalized $\sigma(\omega)$ is plotted together in Fig. 3(d) for 20 nm channels of PEDOT:Tos and PEDOT:PSS. The temperature dependence of the onset frequency, $\omega_0(T)$ where $\sigma(\omega_0) = 1.1 \sigma_{\text{dc}}$, is plotted in the inset of Fig. 3(d) for two different PEDOT systems. The correlation length scale, λ , where $\lambda \propto 1/\omega_0$ corresponds to the path lengths along the conducting polymer network [40,41]. Observations reveal a temperature-independent shorter λ associated with PEDOT:Tos and a temperature-dependent, significantly larger λ for PEDOT:PSS for a temperature variation over $80 \text{ K} < T < 340 \text{ K}$. The temperature-independent s and ω_0 (and λ) trend of PEDOT:Tos emphasizes the negligible thermal disorder of PEDOT:Tos over PEDOT:PSS. These results strongly

relate to the metallicity and the improved order parameter in the PEDOT:Tos system.

D. Electrical noise analysis

Electrical noise characterization is studied to probe the microscopic details of local current inhomogeneities over the bulk resistances [42]. Noise analysis of electrical transport can reveal the extent of disorder in the electronic states. Time-dependent fluctuations in current (noise) provide insight into the energetic landscape traversed by charge carriers [43] and can be analyzed in the ω domain as power spectrum density (PSD) response. Noise fluctuations inversely scale with the conductance in the systems, with PEDOT:PSS exhibiting higher noise amplitudes than PEDOT:Tos channels. This result highlights the higher degree of disorder in PEDOT:PSS [44]. Both the systems exhibited the characteristic $1/f^\gamma$ behavior where Hooge's exponent lies in $1.2 < \gamma < 2$ for PEDOT:PSS and $\gamma \approx 2$ for PEDOT:Tos. However, the noise characteristics showed the following traits: (i) The $1/f^\gamma$ response from the normalized $S_I(\omega)/I^2$ in the case of PEDOT:PSS depended on the dc-current magnitude (controlled by bias) and indicates a dispersive electrical transport behavior [Fig. 4(a)]; (ii) $S_I(\omega)/I^2$ in $153 \text{ K} < T < 400 \text{ K}$ range for PEDOT:PSS shows a variation of three orders of magnitude [Fig. 4(a) for 100 mV] as compared to a largely bias-independent, T -independent $S_I(\omega)/I^2$ noise response from PEDOT:Tos nanochannels [Fig. 4(b)]; (iii) Sweeping through different bias conditions of 100, 500, and 800 mV at

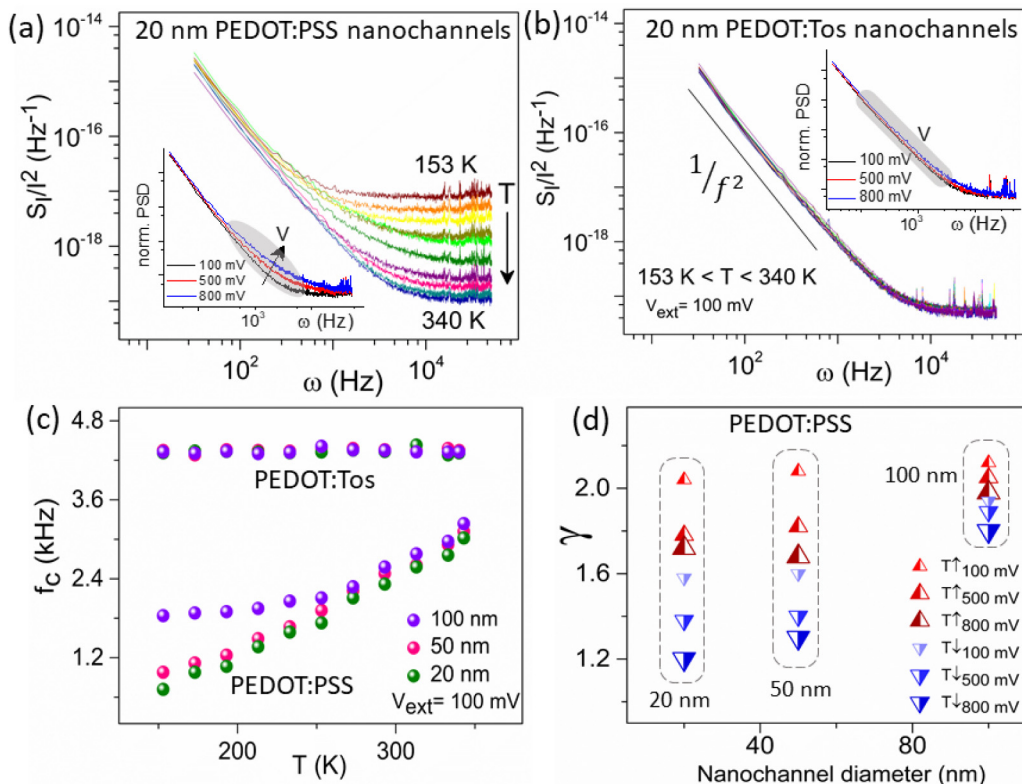


FIG. 4. Noise studies, $S_I(\omega)/I^2$ in (a) 20 nm PEDOT:PSS nanochannels, and (b) 20 nm PEDOT:Tos nanochannels over a temperature range of $153 \text{ K} < T < 340 \text{ K}$, respectively. Insets of (a), (b) show the respective normalized PSD with bias conditions. (c) Corner frequency f_c versus T for PEDOT:PSS and PEDOT:Tos channel dimensions. (d) Hooge's exponent, γ with different bias conditions at max $T \uparrow = 340 \text{ K}$ (red) and min $T \downarrow = 153 \text{ K}$ (blue) as parameters for 20, 50, and 100 nm PEDOT:PSS nanochannels, respectively.

different temperatures there is a decrease in slope $|-dS_I/d\omega|$ with increasing bias [inset of Fig. 4(a) at $T = 313 \text{ K}$], whereas $|-dS_I/d\omega|$ is fairly constant for different bias-voltage conditions in PEDOT:Tos [inset of Fig. 4(b) at $T = 313 \text{ K}$]; (iv) Corner frequency f_c variation with T for different dimensions of PEDOT:PSS nanochannels with 20 nm at 100 mV is most dispersive and PEDOT:Tos nanochannels has nearly no T dependence [Fig. 4(c)]; (v) The range of γ for different bias conditions and T range [$T_{\min} = 153 \text{ K}$ and $T_{\max} = 340 \text{ K}$ in Fig. 4(d)] shows low value of $\gamma \approx 1.2$ for 20 nm channels at high bias $V = 800 \text{ mV}$ and low T . (Noise response from other nanochannel dimensions as a function of V_{ext} and T are shown in Sec. 8 of the Supplemental Material [31].) Extent of dispersion at high ω and low T can also be captured by corner frequency f_c , beyond which an apparent white-noise feature emerges. f_c increases linearly with T for PEDOT:PSS nanochannels, 20 nm at 100 mV being most dispersive (Sec. 8 of the Supplemental Material [31]). The different factors contributing to the measured noise in these systems are quite difficult to resolve. However, a qualitative analogy can be made with impedance studies. The temperature-dependent dispersive behavior of $S_I(\omega)/I^2$ at high ω in the case of PEDOT:PSS is indicative of a stronger temperature dependence of σ as opposed to a weak $\sigma(T)$ behavior in PEDOT:Tos. These characteristic fluctuations in PEDOT:PSS can be correlated to the orientational processes accompanied by a thermal disorder.

III. CONCLUSION

In conclusion, a comparative study of the two CPs, PEDOT:PSS and PEDOT:Tos, confined within nanopores reveals the importance of structural disorder and its role in transport kinetics. The large increase of σ within the nanopore scaffold provides a route to enhance the vertical transport of PEDOT films. The increase in σ by several orders of magnitude is observed to occur for systems where the polymer emerges from *in situ* polymerization of the monomer within the nanochannels as compared to polymers inserted from a solution phase into the channels. The frequency domain σ and time-domain noise studies provide further insight with $\sigma(\omega)$ in disordered PEDOT:PSS exhibiting a power-law behavior and wide dispersion both over ω and T , in contrast to the negligibly varying $\sigma(\omega, T)$ and comparatively less disordered PEDOT:Tos. Based on these studies, the confinement template offers some insight into the role of different dopant environments around an electronic backbone.

ACKNOWLEDGMENTS

We acknowledge K. L. Narasimhan and N. S. Vidhyadhiraja for useful discussions. S.D. thanks A. Sundaresan, D. P. Panda, and M. Shrivastava for use of the low-temperature dc measurement facility. K.S.N. acknowledges support from the DST-JC Bose fellowship.

- [1] P. Sheng, Fluctuation-induced tunneling conduction in disordered materials, *Phys. Rev. B* **21**, 2180 (1980).
- [2] A. B. Kaiser, Electronic transport properties of conducting polymers and carbon nanotubes, *Rep. Prog. Phys.* **64**, 1 (2001).
- [3] A. B. Kaiser and V. Skakalova, Electronic conduction in polymers, carbon nanotubes and graphene, *Chem. Soc. Rev.* **40**, 3786 (2011).
- [4] J. Chung, A. Khot, B. M. Savoie, and B. W. Boudouris, 100th Anniversary of macromolecular science viewpoint: Recent advances and opportunities for mixed ion and charge conducting polymers, *ACS Macro Lett.* **9**, 646 (2020).
- [5] M. N. Gueye, A. Carella, J. Faure-Vincent, R. Demadrille, and J.-P. Simonato, Progress in understanding structure and transport properties of PEDOT-based materials: A critical review, *Prog. Mater. Sci.* **108**, 100616 (2020).
- [6] M. Jaiswal and R. Menon, Polymer electronic materials: A review of charge transport, *Polym. Int.* **55**, 1371 (2006).
- [7] P. W. Anderson, Absence of diffusion in certain random lattices, *Phys. Rev.* **109**, 1492 (1958).
- [8] P. Pingel, A. Zen, R. D. Abellón, F. C. Grozema, L. D. Siebbeles, and D. Neher, Temperature-resolved local and macroscopic charge carrier transport in thin P3HT layers, *Adv. Funct. Mater.* **20**, 2286 (2010).
- [9] R. Noriega, J. Rivnay, K. Vandewal, F. P. Koch, N. Stingelin, P. Smith, M. F. Toney, and A. Salleo, A general relationship between disorder, aggregation and charge transport in conjugated polymers, *Nat. Mater.* **12**, 1038 (2013).
- [10] A. Zen, M. Saphiannikova, D. Neher, J. Grenzer, S. Grigorian, U. Pietsch, U. Asawapirom, S. Janietz, U. Scherf, and I. Lieberwirth, Effect of molecular weight on the structure and crystallinity of poly(3-hexylthiophene), *Macromolecules* **39**, 2162 (2006).
- [11] N. Rolland, J. F. Franco-Gonzalez, R. Volpi, M. Linares, and I. V. Zozoulenko, Understanding morphology-mobility dependence in PEDOT:Tos, *Phys. Rev. Mater.* **2**, 045605 (2018).
- [12] H. Shi, C. Liu, Q. Jiang, and J. Xu, Effective approaches to improve the electrical conductivity of PEDOT:PSS: A review, *Adv. Electron. Mater.* **1**, 1500017 (2015).
- [13] J. Kim, J. Jung, D. Lee, and J. Joo, Enhancement of electrical conductivity of poly(3,4-ethylenedioxythiophene)/poly(4-styrenesulfonate) by a change of solvents, *Synth. Met.* **126**, 311 (2002).
- [14] N. Kim, H. Kang, J. H. Lee, S. Kee, S. H. Lee, and K. Lee, Highly conductive all-plastic electrodes fabricated using a novel chemically controlled transfer-printing method, *Adv. Mater.* **27**, 2317 (2015).
- [15] J. M. D'Arcy, M. F. El-Kady, P. P. Khine, L. Zhang, S. H. Lee, N. R. Davis, D. S. Liu, M. T. Yeung, S. Y. Kim, and C. L. Turner, Vapor-phase polymerization of nanofibrillar poly(3,4-ethylenedioxythiophene) for supercapacitors, *ACS Nano* **8**, 1500 (2014).
- [16] O. Bubnova, Z. U. Khan, H. Wang, S. Braun, D. R. Evans, M. Fabretto, P. Hojati-Talemi, D. Dagnelund, J.-B. Arlin, and Y. H. Geerts, Semi-metallic polymers, *Nat. Mater.* **13**, 190 (2014).
- [17] N. Kim, B. H. Lee, D. Choi, G. Kim, H. Kim, J.-R. Kim, J. Lee, Y. H. Kahng, and K. Lee, Role of Interchain Coupling in the Metallic State of Conducting Polymers, *Phys. Rev. Lett.* **109**, 106405 (2012).
- [18] A. Elschner, S. Kirchmeyer, W. Lovenich, U. Merker, and K. Reuter, *PEDOT: Principles and Applications of an Intrinsically Conductive Polymer* (CRC Press, Boca Raton, FL, 2010).
- [19] M. J. Donahue, A. Sanchez-Sanchez, S. Inal, J. Qu, R. M. Owens, D. Mecerreyes, G. G. Malliaras, and D. C. Martin, Tailoring PEDOT properties for applications in bioelectronics, *Mater. Sci. Eng., R* **140**, 100546 (2020).
- [20] W.-S. Tung, R. J. Composto, R. A. Riggelman, and K. I. Winey, Local polymer dynamics and diffusion in cylindrical nanoconfinement, *Macromolecules* **48**, 2324 (2015).
- [21] S. Cho, S. Jeong, J. M. Kim, and C. Baig, Molecular dynamics for linear polymer melts in bulk and confined systems under shear flow, *Sci. Rep.* **7**, 9004 (2017).
- [22] M. A. Leaf and M. Muthukumar, Electrostatic effect on the solution structure and dynamics of PEDOT:PSS, *Macromolecules* **49**, 4286 (2016).
- [23] U. Lang, E. Müller, N. Naujoks, and J. Dual, Microscopical investigations of PEDOT:PSS thin films, *Adv. Funct. Mater.* **19**, 1215 (2009).
- [24] Y. Xia, K. Sun, and J. Ouyang, Solution-processed metallic conducting polymer films as transparent electrode of optoelectronic devices, *Adv. Mater.* **24**, 2436 (2012).
- [25] Q. Wei, M. Mukaida, Y. Naitoh, and T. Ishida, Morphological change and mobility enhancement in PEDOT:PSS by adding co-solvents, *Adv. Mater.* **25**, 2831 (2013).
- [26] B. Cho, K. S. Park, J. Baek, H. S. Oh, Y.-E. Koo Lee, and M.M. Sung, Single-crystal poly(3,4-ethylenedioxythiophene) nanowires with ultrahigh conductivity, *Nano Lett.* **14**, 3321 (2014).
- [27] O. Bubnova, Z. U. Khan, A. Malti, S. Braun, M. Fahlman, M. Berggren, and X. Crispin, Optimization of the thermoelectric figure of merit in the conducting polymer poly(3,4-ethylenedioxythiophene), *Nat. Mater.* **10**, 429 (2011).
- [28] M. Upadhyaya, C. J. Boyle, D. Venkataraman, and Z. Aksamija, Effects of disorder on thermoelectric properties of semiconducting polymers, *Sci. Rep.* **9**, 5820 (2019).
- [29] K. Aasmundtveit, E. Samuelsen, L. Pettersson, O. Inganäs, T. Johansson, and R. Feidenhans, Structure of thin films of poly(3,4-ethylenedioxythiophene), *Synth. Met.* **101**, 561 (1999).
- [30] S. Das and K. S. Narayan, Significant increase in electrical transport of conducting polymers confined in alumina nanopores, *J. Phys. Chem. C* **123**, 11284 (2019).
- [31] See Supplemental Material at <http://link.aps.org/supplemental/10.1103/PhysRevMaterials.6.025602> for experimental methods, experiments showing complete filling of nanochannel with the polymer, noncontact mode surface morphology of PEDOT:Tos nanochannels, contact mode current imaging of PEDOT:Tos nanochannels, for PEDOT:Tos nanochannels (linear scale), PEDOT crystalline domains, ac conductivity $\sigma(\omega, T)$ of PEDOT:Tos nanochannels, and electrical noise analysis.
- [32] Z. U. Khan, O. Bubnova, M. J. Jafari, R. Brooke, X. Liu, R. Gabrielsson, T. Ederth, D. R. Evans, J. W. Andreasen, and M. Fahlman, Acido-basic control of the thermoelectric properties of poly(3,4-ethylenedioxythiophene) tosylate (PEDOT-Tos) thin films, *J. Mater. Chem. C* **3**, 10616 (2015).
- [33] K. Swathi and K. Narayan, Self-assembled porous alumina based organic nanotriode arrays, *Nano Lett.* **17**, 7945 (2017).
- [34] R. Harsh and K. Narayan, Noise spectroscopy of polymer transistors, *J. Appl. Phys.* **118**, 205502 (2015).

- [35] S. Chen, I. Petsagkourakis, N. Spampinato, C. Kuang, X. Liu, R. Brooke, E. S. Kang, M. Fahlman, X. Crispin, and E. Pavlopoulou, Unraveling vertical inhomogeneity in vapour phase polymerized PEDOT:Tos films, *J. Mater. Chem. A* **8**, 18726 (2020).
- [36] R. Menon, C. Yoon, D. Moses, A. Heeger, and Y. Cao, Transport in polyaniline near the critical regime of the metal-insulator transition, *Phys. Rev. B* **48**, 17685 (1993).
- [37] C. S. S. Sangeeth, M. Jaiswal, and R. Menon, Correlation of morphology and charge transport in poly(3,4-ethylenedioxythiophene)-polystyrenesulfonic acid (PEDOT-PSS) films, *J. Phys.: Condens. Matter* **21**, 072101 (2009).
- [38] A. M. Nardes, M. Kemerink, and R. A. J. Janssen, Anisotropic hopping conduction in spin-coated PEDOT:PSS thin films, *Phys. Rev. B* **76**, 085208 (2007).
- [39] A. Kaiser, Metallic behaviour in highly conducting polymers, *Synth. Met.* **45**, 183 (1991).
- [40] B. E. Kilbride, J. Coleman, J. Fraysse, P. Fournet, M. Cadek, A. Drury, S. Hutzler, S. Roth, and W. Blau, Experimental observation of scaling laws for alternating current and direct current conductivity in polymer-carbon nanotube composite thin films, *J. Appl. Phys.* **92**, 4024 (2002).
- [41] A. Papathanassiou, I. Sakellis, and J. Grammatikakis, Universal frequency-dependent ac conductivity of conducting polymer networks, *Appl. Phys. Lett.* **91**, 122911 (2007).
- [42] J. Planès and A. François, Percolation scaling, inhomogeneity, and defects in polyaniline blends: A $1/f$ noise diagnosis, *Phys. Rev. B* **70**, 184203 (2004).
- [43] P. Dutta, P. Dimon, and P. Horn, Energy Scales for Noise Processes in Metals, *Phys. Rev. Lett.* **43**, 646 (1979).
- [44] S. Shekhar, D. Cho, H. Lee, D.-g. Cho, and S. Hong, Nanoscale direct mapping of localized and induced noise sources on conducting polymer films, *Nanoscale* **8**, 835 (2016).